The dynamics and stability of lubricating oil films during droplet transport by electrowetting in microfluidic devices

Jairus Kleinert,[1,2,a)] Vijay Srinivasan,[1,b)] Arnaud Rival,[3] Cyril Delattre,[3] Orlin D. Velev,[2] and Vamsee K. Pamula[1,b),c)]
[1]*Advanced Liquid Logic, Inc., PO Box 14025, Research Triangle Park, North Carolina 27709, USA*
[2]*Department of Chemical and Biomolecular Engineering, North Carolina State University, Raleigh, North Carolina 27695-7905, USA*
[3]*Advanced Liquid Logic France, MINATEC – BHT – Bat 52, 7 parvis Louis Néel, 38000 Grenoble, France*

(Received 8 March 2015; accepted 11 May 2015; published online 19 May 2015)

The operation of digital microfluidic devices with water droplets manipulated by electrowetting is critically dependent on the static and dynamic stability and lubrication properties of the oil films that separate the droplets from the solid surfaces. The factors determining the stability of the films and preventing surface fouling in such systems are not yet thoroughly understood and were experimentally investigated in this study. The experiments were performed using a standard digital microfluidic cartridge in which water droplets enclosed in a thin, oil-filled gap were transported over an array of electrodes. Stable, continuous oil films separated the droplets from the surfaces when the droplets were stationary. During droplet transport, capillary waves formed in the films on the electrode surfaces as the oil menisci receded. The waves evolved into dome-shaped oil lenses. Droplet deformation and oil displacement caused the films at the surface opposite the electrode array to transform into dimples of oil trapped over the centers of the droplets. Lower actuation voltages were associated with slower film thinning and formation of fewer, but larger, oil lenses. Lower ac frequencies induced oscillations in the droplets that caused the films to rupture. Films were also destabilized by addition of surfactants to the oil or droplet phases. Such a comprehensive understanding of the oil film behavior will enable more robust electrowetting-actuated lab-on-a-chip devices through prevention of loss of species from droplets and contamination of surfaces at points where films may break.
[http://dx.doi.org/10.1063/1.4921489]

I. INTRODUCTION

The concept of digital microfluidics (DMF), in which discrete droplets are individually manipulated in an open structure using electric fields, is an alternative with distinct advantages to the closed-channel, continuous-flow type of microfluidics devices.[1–4] In DMF systems, each droplet functions as an independent liquid container or reactor, enabling many parallel operations. Droplets can be transported, split, and merged in a highly controlled manner[5] to perform assay protocols, which can be readily modified by changing the composition and sequence of droplets, without altering the device itself. A wide range of chemical and biochemical operations including chemical detection, synthesis, enzymatic assays, immunoassays, PCR, hybridization and sequencing of DNA, and cell culture have been implemented in DMF devices.[2,4]

[a)]Present address: Illumina, Inc., 5200 Illumina Way, San Diego, California 92122, USA.
[b)]Present address: Baebies, Inc., PO Box 14403, Durham, North Carolina 27709, USA.
[c)]Author to whom correspondence should be addressed. Electronic mail: vpamula@baebies.com.

A common type of DMF device uses electrowetting to produce and control droplets confined in two dimensions in a flow system without channel walls.[6,7] Electrowetting is an effect by which a droplet spreads on a hydrophobic layer of dielectric material when a voltage is applied between an electrode in contact with the droplet and one beneath the thin insulator. The electric field engenders charges at the dielectric surface, lowering the interfacial energy, and the apparent contact angle of the droplet.[8] Microfluidic devices operating by electrowetting typically consist of two parallel conducting plates separated by a narrow gap. The conductive layer on the bottom plate is patterned into an array of individually addressable electrodes and is covered by a hydrophobic dielectric coating while the opposing top plate has a continuous conductive coating that is hydrophobized. A droplet sandwiched between the two plates can be transported over the array by switching on an electrode adjacent to the droplet, causing the droplet to spread onto the newly charged surface, while simultaneously switching off the electrode directly under the droplet.[6] The droplets are commonly manipulated in a continuous phase of immiscible oil. The oil has several roles, including maintaining spacing between the droplets,[9] preventing droplet evaporation,[10] lubricating droplet motion,[10,11] and inhibiting molecular transfer between droplets and adsorption from droplets to device surfaces.[4,10,12] Consequently, the stability of the fragile thin film of oil that forms between the droplets and device surfaces is critical to reliable device operation.

The dynamics of thin films between solid surfaces and tangentially moving fluid interfaces in pressure-driven flow systems have been modeled previously by other researchers. Foremost among them are Landau and Levich,[13] who described the liquid film formed on a flat plate vertically withdrawn from a liquid bath, and Bretherton,[14] who examined the film surrounding a bubble moving through a liquid-filled capillary. Both theories predict that the film thickness h is governed by the equation

$$h = 1.34\,R\,Ca^{2/3}, \tag{1}$$

in which R is the radius of curvature of the meniscus and Ca is the capillary number, which depends on the viscosity of the liquid in the film μ, the speed at which the meniscus recedes U, and the surface tension of the liquid γ through the relation

$$\mathrm{Ca} = \frac{\mu U}{\gamma}. \tag{2}$$

The height of a precursor film spreading from a sessile droplet has also been shown to follow a similar relation to Ca.[15]

The Landau-Levich and Bretherton models rely on the assumptions that the free surface of the film is in air and free of surfactant. However, these assumptions do not necessarily apply in DMF systems which contain a second liquid phase instead of air and often include surfactants as components of biological assays. The higher viscosity of the droplets compared to air means that shear stresses arising from flows inside the droplets are large enough to entrain liquid and increase the film thickness.[16,17] During droplet motion, surfactants adsorbed to the free surface of the film accumulate at the leading end of the droplet and become depleted in the adjacent region of the film. The lower interfacial tension in the droplet cap relative to the film creates a Marangoni stress that thickens the film.[18] However, the surfactants affect the film thickness only at low concentrations[18] or if adsorption to the interface is slow.[19] Fast diffusion of molecules from the bulk to the depletion zone at high surfactant concentrations coupled to rapid adsorption or surface convection diminish the concentration gradient.[19,20] The increases in film thickness caused by droplet viscosity and surfactant redistribution can be accounted for by increasing the constant in Eq. (1).[16–18]

The thickness and stability of oil films around droplets actuated by electrowetting have not yet been extensively investigated. A theoretical analysis considered the effect of electrowetting on an oil layer of less than 400 nm thickness completely covering a dielectric substrate in an aqueous medium.[21] According to this study, when a voltage is applied across the system, the

film transitions to a pseudo-partial wetting state—a 25 nm thin oil film supported by van der Waals interactions existing in equilibrium with a macroscopic oil droplet—and is not displaced by complete wetting of the substrate by the aqueous phase. For films of higher initial thickness, the model anticipates that the electrostatic pressure engendered by the voltage may lead to spinodal dewetting, whereby capillary waves arise at the fluid interface and lead to break up of the film. Consistent with that prediction, an experimental investigation showed that an oil film entrapped by a water droplet expanding radially by electrowetting over a dielectric substrate dewets into an array of discrete oil droplets when the equilibrium electrowetting radius is reached.[22] In this work, the speed of the droplet spreading and the oil meniscus receding was varied by adjusting the rate at which the voltage was increased from zero to a fixed value, and the thickness of the entrapped film was found to follow a relationship similar to the Landau-Levich dipcoating model[13] modified to account for the electrostatic pressure. The oil droplet diameters were correlated to the wavelengths of variations in film thickness predicted by a linear stability analysis. The study suggests that the film behavior is governed by the dynamics of the receding oil meniscus.

While the previous investigations have provided some insight into the behavior of oil films during electrowetting, the systems that were examined are different from DMF devices in several aspects that influence the film dynamics and stability. The apparatus used in the earlier experiments consisted of a spherical water droplet sitting in oil on a dielectric substrate. As the voltage was gradually increased, the droplet spread symmetrically over the substrate, entrapping oil, and forming a film, while the center of the droplet remained stationary. The droplets in practical DMF devices are confined between two parallel surfaces and are, thus, disk-shaped with oil films between the flattened droplet surfaces and the device surfaces. When an electrode adjacent to a droplet is activated, the droplet asymmetrically wets the electrode, and its center moves laterally to the middle of the electrode. The voltage is applied as a step in contrast to the earlier experiments in which the voltage was ramped, increasing the speed at which the oil meniscus recedes, a critical parameter governing the film thickness. While the previous studies examined only the films at the dielectric-covered bottom surface, where electrowetting drives droplet spreading, droplet actuation affects the films differently at the top surface lacking a dielectric layer, where the electrowetting effect is weak.

In this article, we report an investigation of the dynamics and stability of oil films in the geometry and actuation scheme that is specific to DMF devices. We first present experimental observations and measurements of the characteristic features and behaviors of oil films above and below static droplets confined in the devices, laterally immobile droplets subjected to electrowetting, and droplets transported by electrowetting along paths of electrodes. Next, we describe the effects on the films of modifying the electric field and frequency, as well as adding surfactants, which are almost always present in chemical or biochemical analytical systems. In Sec. V, we provide a semi-quantitative analysis of the observed film stability and properties and explain how the resulting understanding of oil film behavior in DMF systems can be used to design devices with improved performance.

II. MATERIALS AND METHODS

The DMF device used in the experiments was representative of commercial systems. It consisted of two main components: a cartridge in which droplets in a narrow, oil-filled gap between two parallel plates were moved in two dimensions by electrowetting and a computer-programmable electronic circuit that controlled the voltage applied to each electrode in the cartridge to cause droplets to undergo a user-defined sequence of actions. The oil films between the droplets and the cartridge surfaces were observed by interference microscopy. The technical details of all components are presented below.

A. Cartridge construction

The cartridges, depicted in Figure 1, were made from two glass plates coated on one side with a conductive layer of indium tin oxide. The optically transparent plates permitted

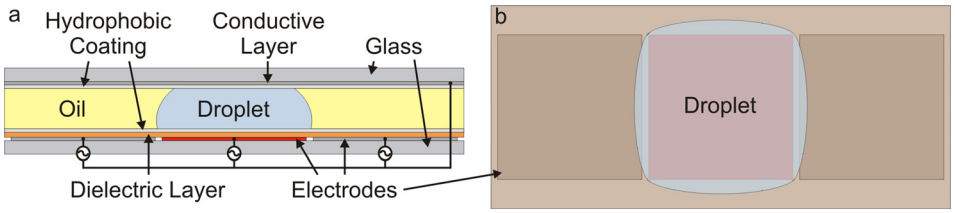

FIG. 1. Schematic illustrating (a) a side view and (b) a top view of a portion of an electrowetting-actuated DMF device. Droplets were confined to an oil-filled slit between a top plate and a bottom plate featuring an array of electrodes. Upon application of voltage at a specific electrode (shown in red), a droplet moved from an adjacent electrode onto the activated electrode by electrowetting.

microscopic observation of the oil films inside the cartridges. The bottom plate functioned as the working electrode surface and was laminated with a 0.5 mil thick polyimide film which formed the dielectric layer necessary for electrowetting. The film was applied to the glass plate using a roll laminator at a speed of 30 cm/min. The top plate, termed the reference surface, contacted the droplet directly to complete the circuit. Both plates were hydrophobized by a 150 nm thick coating of CYTOP fluoropolymer. The hydrophobic coating was deposited by immersing the slide in a solution of CYTOP for 10 s and withdrawing it at a rate of 100 mm/min using a linear motor.

Two versions of the working electrode plate were fabricated. One type featured a continuous conductive layer and was used to make cartridges in which the droplets remained stationary and were subject to radially symmetrical electrowetting. The conductive layer of the other type was patterned by standard photolithography and wet etching processes to create an array of electrodes each the same size as the footprint of a droplet, enabling lateral transport of a droplet through the cartridge by sequential application of voltage to electrodes in a row. Each plate had five parallel rows of ten 1 mm × 1 mm electrodes and 2 mm × 3 mm reservoir electrodes at both ends of each row. The two types of cartridges allowed the effects of electrostatic pressure and droplet motion on the oil films to be studied independently.

After coating, the two plates were placed with the conductive sides facing each other and separated by a 300 μm plastic spacer. The assembly was held together by microscope stage clips, and the gap between the plates was filled with silicone oil. On the cartridges designed for stationary electrowetting, a 300 nl water droplet was deposited into the oil using a pipette. On the cartridges designed for lateral transport of droplets, several microliters of water were loaded through holes drilled in the top plates over the reservoir electrodes, and droplets were dispensed from the reservoirs using previously described electrode actuation sequences.[5] A new cartridge was used for each experiment.

B. Liquid phase materials

The silicone oil used to fill the cartridges was 2 cSt trimethylsiloxy-terminated poly(dimethylsiloxane) (PDMS) from Gelest (Morrisville, PA). The droplets were deionized water to which potassium chloride was added at a concentration of 100 mM to ensure good conductivity as required for electrowetting. To study the effects of surfactants on the oil films, Tween 20 or Triton X-15 from Sigma-Aldrich (St. Louis, MO) was added to the droplet or oil phase, respectively. Surfactants are often classified by hydrophilic-lipophilic balance (HLB), a scale ranging from 0 to 20 on which 0 indicates a water-insoluble molecule and 20 indicates a lipid-insoluble molecule. Tween 20, commonly used in buffers for biochemical assays, has an HLB of 16.7, while Triton X-15 has an HLB of 4.9.

C. Electrical instrumentation

Voltage was supplied to each electrode on the cartridge by a computer-controlled circuit designed and built by Advanced Liquid Logic (Research Triangle Park, NC) for commercial DMF products. The hardware was modified to allow the cartridges to fit on a microscope stage.

Switching of the voltage to the electrodes was programmed and executed using software developed by Advanced Liquid Logic. For all experiments, except where stated otherwise, droplets were manipulated using a square wave voltage of 275 V at a frequency of 100 Hz.

D. Characterization

The oil films between droplets and cartridge surfaces were examined by interference microscopy using an Olympus BX41 microscope operating in reflected light mode. A 550 nm bandpass filter was placed in the illuminating light path to provide a monochromatic beam. The films were observed through 10×, 20×, and 40× objectives, and images and videos were recorded using a CV-S3200 camera from JAI (Kushima City, Japan) connected to a PC running DScaler open-source software. Side-view, slow-motion videos of droplet transport were recorded using an EoSens mini2 camera from Mikrotron (Unterschleissheim, Germany) at a frame rate of 2500 fps and 10× magnification.

The interfacial tensions between the oil and droplet phases at different concentrations of surfactants were measured using a CAM 101 goniometer from KSV (Espoo, Finland). Droplets of the water phase were held at the tip of a needle immersed in the oil phase for 2 min to allow the surfactant concentration at the droplet surface to reach equilibrium. Then, ten images of each droplet were recorded at 3 s intervals. The interfacial tension was calculated based on the shapes of the droplets in the images by an algorithm in the software provided with the instrument.

III. RESULTS

A. Observation and characterization of oil films above and below stationary droplets

Oil films were initially observed immediately after loading droplets into cartridges and before applying voltage. An example of an interferogram of a film formed where a droplet was pressed flat against a cartridge surface is shown in Figure 2. The image is typical of 20 such static films observed on 5 different cartridges. The bright and dark patterns in the film appeared because the monochromatic light waves reflected from the cartridge surface and the oil-droplet interface interfered alternatingly constructively and destructively as the film thickness varied. The thicknesses at specific points in the films were calculated using the equation

$$h = \frac{\lambda}{2\,\pi\, n_f}\left(l\,\pi \pm \arcsin\sqrt{\Delta I}\right), \tag{3}$$

where λ is the wavelength of the light, n_f is the refractive index of the oil, and l is the order of interference.[23] The relative light intensity ΔI was calculated by

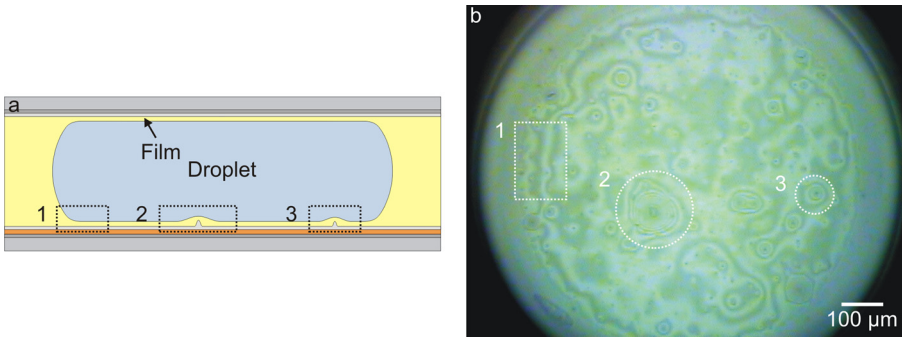

FIG. 2. (a) Schematic and (b) interference micrograph showing a thin film between a droplet and cartridge surface before voltage was applied. (1) The broadening interference bands around the edge of the film showed a transition from an oil meniscus to a thin film rather than a three-phase contact line. (2) and (3) Oil lenses, circular regions where the film was thicker, appeared towards the center of the film.

$$\Delta I = \frac{I_{max} - I}{I_{max} - I_{min}}, \tag{4}$$

where I_{max} and I_{min} are the maximum and minimum light intensity in a film and I is the light intensity at the point where the thickness is to be determined. For the system in this study, $\lambda = 550$ nm, $n_f = 1.39$, and the difference in the film thickness between two adjacent interference maxima or minima was 198 nm. The resolution of the film thickness measurement depended upon the ability to distinguish different levels of light intensity in the interference micrographs and, for the present implementation, was estimated to be 3–4 nm based on 25–35 levels of light intensity between adjacent dark and bright interference fringes in typical images from the experiments in this study. The depth of field of the microscope was sufficiently small that the interference patterns from the film could be distinguished from those from the cartridge coatings.

The appearance of interference patterns across the flattened area of the droplet showed that the oil film was continuous with varying thickness. The broadening bands encircling the inside edge of the film, as shown in box 1 of Figures 2(a) and 2(b), suggested a transition from the oil meniscus surrounding the droplet to a thin oil film rather than a contact line bounding the oil phase. The smoothness of the surfaces was likely to contribute to the film stability. Contact profilometry measurements of cartridge surfaces indicated average roughness varying from 6.4 to 14.9 nm, smaller than the expected oil film thickness. Larger features that approached the height of the film might have imposed points of high curvature on the droplet surface, creating capillary pressure gradients that could have drained the film. Nevertheless, the interference patterns did show concentric rings of more closely spaced fringes towards the center of the droplet, as shown in boxes 2 and 3, that indicated dome-shaped lenses of oil where the film thickened to accommodate microscale objects such as dust particles. The large areas of uniform intensity corresponded to flat, thin films. Equations (3) and (4), along with λ and n_f stated above, were used to estimate the thickness of the flat areas of films by comparing the light intensity I in these regions to the darkest and brightest points I_{min} and I_{max} in the same images. In order to know the absolute film thickness, the order of interference must also be determined, typically by counting the number of interference fringes between the measurement point and an area of the substrate not covered by the film. However, there was no reference point where the film was broken and the substrate exposed in the DMF system observed here. Thus, the flat areas of the film were assumed to be in the lowest order of interference, and the film was estimated to be less than 50 nm thick in these areas. The film remained static as long as it was not perturbed.

B. Observation and characterization of oil films formed during stationary-droplet electrowetting

In the next experiments, the dynamics of oil films were observed when voltage was applied at 275 V and 100 Hz to cause electrowetting of stationary droplets. The experiments were performed using cartridges with a single, large working electrode, as illustrated in the schematics in Figures 3(a) and 3(b). When the voltage was switched on, the film thinned at both the reference surface and the working electrode surface. The oil from both films was displaced into lenses that formed throughout the films, as seen on the right side of each of the interferograms in Figures 3(c)–3(f). In addition to thinning, the oil film at the working electrode surface expanded in area as the electrowetting effect caused the droplet to spread. Waves formed concentrically at the receding oil meniscus, arising from competition between interfacial, electrostatic, and hydrodynamic energies as oil was displaced from around the spreading droplet into the newly created film. The waves evolved into oil lenses, as shown in the boxes in Figures 3(d)–3(f). This film behavior was observed upon repeated actuations of droplets on 3 different cartridges. At the reference surface, the area of the film was reduced as the shape of the droplet changed to compensate for the spreading at the working electrode surface. When the voltage

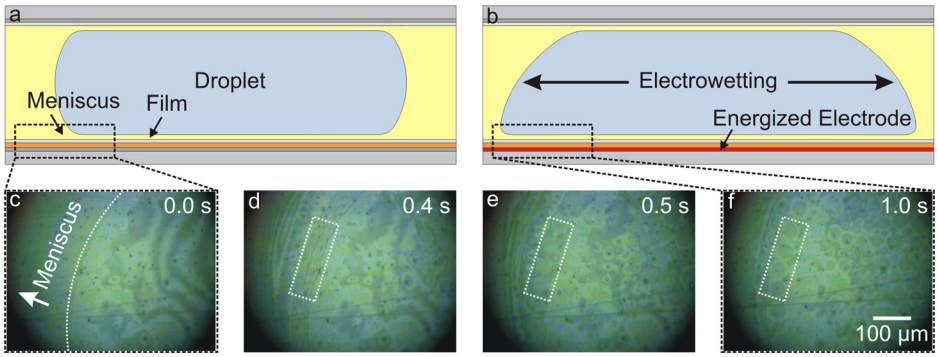

FIG. 3. (a) and (b) Schematics and (c) and (f) interference micrographs showing the evolution of an oil film between a stationary droplet and the working electrode surface after voltage was applied at 275 V and 100 Hz. (a) Initially, the droplet was symmetrical at the top and bottom surfaces of the cartridge. (b) When the voltage was applied, the droplet spread to cover more of the surface of the dielectric layer on the working electrode. (c)–(f) Waves formed in the film at the receding oil meniscus and developed into circular oil lenses, as shown in the dotted box. Oil was displaced into lenses in the center of the film.

was switched off, the droplet and films returned to their original shapes and sizes, and the oil lenses flattened.

C. Observation and characterization of oil films during electrowetting-driven droplet transport

Next, the dynamics of oil films were characterized during electrowetting-driven translational droplet motion using the cartridges with patterned working electrode arrays. Films were observed during transport of droplets forward and backward along rows of electrodes at 275 V and 100 Hz on 3 different cartridges. A droplet was transported by switching off the electrode under the droplet, while simultaneously switching on an adjacent electrode. As the droplet wetted the activated electrode and dewetted the deactivated electrode, it briefly adopted an elongated shape with the top pulled away from the reference surface, as shown in frames from a side-view recording of droplet transport in Figures 4(a)–4(c) and illustrated in Figures 4(d) and 4(e). Upon completing movement onto the activated electrode, the droplet returned to a circular shape and reapproached the top of the cartridge. The perimeter of the droplet was pressed flat against the cartridge surface, forming a barrier and entrapping a dimple of oil above the center of the droplet, as shown in Figures 4(f)–4(i). The ring surrounding the dimple contained many small, irregularly shaped, and randomly positioned oil lenses.

At the working electrode surface, as the droplet spread to wet the energized electrode, waves trailed the receding oil meniscus and transformed into circular oil lenses uniformly distributed over the newly formed film, as shown in Figures 4(j)–4(m). The phenomenon was similar to the formation of lenses in the perimeter of an oil film under a stationary droplet subjected to electrowetting as described in Sec. III B. The interferograms were not sufficiently clear to determine if the film between the lenses became very thin or completely dewetted from the cartridge surface. After an initial period of a few seconds during which the oil film evolved, the size and distribution of the lenses in the film remained uniform and constant as long as the electrode remained activated. The appearance of the films did not change for as long as they were observed during the experiments, up to 10 min. The lenses flattened and disappeared if the voltage was removed.

D. Effects of voltage magnitude and frequency

The magnitude and frequency of the ac voltage used to transport droplets had a strong effect on the oil films and were investigated separately. In the experiments described in Secs. III B and III C, a 100 Hz square wave with amplitude of 275 V, the maximum of the voltage source, was used to drive electrowetting. In the next experiments, the amplitude was reduced to

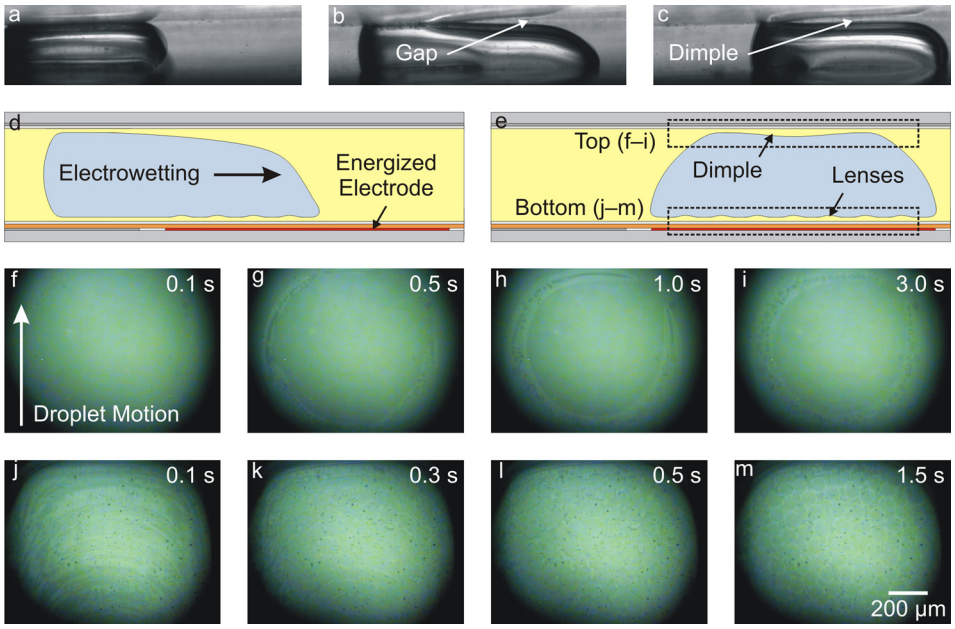

FIG. 4. (a)–(c) Side-view images, (d) and (e) side-view schematics, and (f)–(m) top-view interference micrographs showing the evolution of (a)–(e) the droplet shape and (d)–(m) the oil films as a droplet was transported along a row of discrete electrodes by electrowetting at 275 V and 100 Hz. (b) and (d) When an electrode adjacent to a droplet was switched on, the droplet spread to wet the dielectric layer over that electrode, causing the top of the droplet to be pulled away from the cartridge surface and allowing oil to fill the resulting gap. (c) and (e)–(i) As the droplet motion completed, oil became trapped by the droplet reapproaching the reference surface, and a dimple formed. (d), (e), and (j)–(m) At the working electrode surface, waves formed in the film as the oil meniscus receded and evolved into stable circular oil lenses.

100 V, the minimum at which droplet transport could be achieved, 175 V, or 225 V. Independently, the frequency was adjusted to 10 Hz or 1000 Hz while maintaining the amplitude at 275 V. Oil films at the reference and working electrode surfaces were observed while moving a droplet forward and backward along an electrode path on one cartridge at each pair of voltage settings. The distinctive behaviors at 100 V and 10 Hz were confirmed with repeated experiments on 2–3 cartridges.

The motion of the droplets and the evolution of the oil films occurred more slowly as the magnitude of the voltage decreased, and the oil lenses that formed at the working electrode surface were larger and fewer in number. Table I lists the approximate droplet transport speed, film evolution time, and average oil lens diameter for each amplitude tested, along with *Ca* and *Ew*, the electrowetting number, for each condition. The electrowetting number is the ratio of the electrical energy from applying voltage across the system to the surface energy of the droplet and is given by

$$Ew = \frac{\varepsilon\,\varepsilon_0\,V^2}{2\,d\,\gamma_{OW}}, \tag{5}$$

where ε_d and d are the dielectric constant and thickness of the dielectric layer covering the working electrode surface, V is the applied voltage, and γ_{OW} is the oil-water interfacial energy. At 175 V and 225 V, the film evolution followed the same pattern described in Sec. III C for the experiments at 275 V, but slower evolution of the system and larger areas between the lenses allowed clearer observation of the film dynamics. Interference bands appeared between the lenses as they formed, indicating that a continuous oil film connected them. As the lenses evolved to their final shapes and sizes, the interference fringes between them faded and disappeared one by one until the light intensity was uniform. The interference patterns did not indicate any abrupt change in film thickness between the oil lenses that could be associated with

TABLE I. Effect of voltage magnitude and frequency on droplet transport and oil film evolution.

Voltage (V)	AC frequency (Hz)	Translational droplet speed (mm/s)	*Ca*	*Ew*	Film evolution time (s)	Average oil lens diameter (μm)
100	100	1.5	0.057	0.23	61.0	332
175	100	2.8	0.11	0.71	17.4	179
225	100	4.1	0.16	1.2	4.7	128
275	10	17.1	0.65	1.8	2.1	57
275	100	17.1	0.65	1.8	1.4	65
275	1000	20.0	0.76	1.8	1.6	66

the formation of a contact line and thus did not lead to a conclusive determination about whether the film ruptured or became very thin and flat.

The droplets moved most slowly when actuated at 100 V, and the film dynamics were qualitatively different compared to actuation at higher voltages. At the reference surface, the dimple of oil that formed over the center of the droplet was small, as shown in Figures 5(a), 5(c), and 5(d). The formation of waves at the working electrode surface was not apparent. Rather, broad interference bands encircled the center of the film as the droplet moved. After the droplet stopped, the film thinned slowly, and the oil drained into a large central lens, as shown in Figures 5(b), 5(e), and 5(f). The interference patterns persisted across the film even when the equilibrium state was reached, indicating that the oil film remained intact.

As the frequency of the ac voltage applied to drive electrowetting was reduced to 10 Hz, the oil films became unstable. The evolution of the films was indistinguishable at 100 Hz and 1000 Hz and matched the description in the preceding paragraphs. At 10 Hz, the film behavior also appeared consistent with the previous description while the droplets were in motion. However, when the droplets stopped moving, they began to oscillate with the ac frequency. The vibrations caused the dimple of oil at the reference surface to be ejected into the oil meniscus, as shown in Figures 6(a), 6(c), and 6(d). The oil lenses in the film at the working electrode also vibrated and merged together, as shown in Figures 6(b), 6(e), and 6(f). When the voltage was switched off, the lenses retained their shapes instead of returning to a flat film.

E. Effects of surfactants

Addition of surfactants to either the droplet phase or the oil phase also destabilized the oil films. The films were examined when Tween 20 was added to the droplets at concentrations ranging from 0.0003 to 10.0% (w/v) or Triton X-15 was added to the oil at concentrations

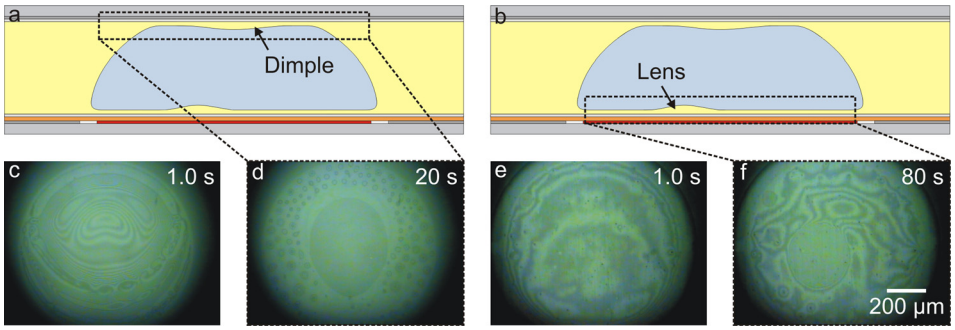

FIG. 5. (a) and (b) Schematics and (c)–(f) interference micrographs showing the evolution of the oil films at (a), (c), and (d) the reference and (b), (e), and (f) the working electrode surfaces when droplets were transported at 100 V. The droplets moved more slowly at 100 V compared to the 275 V used in other experiments. (a), (c), and (d) The dimple that formed at the reference surface was small. (b), (e), and (f) The film at the working electrode surface thinned more slowly, and only a single large oil lens formed.

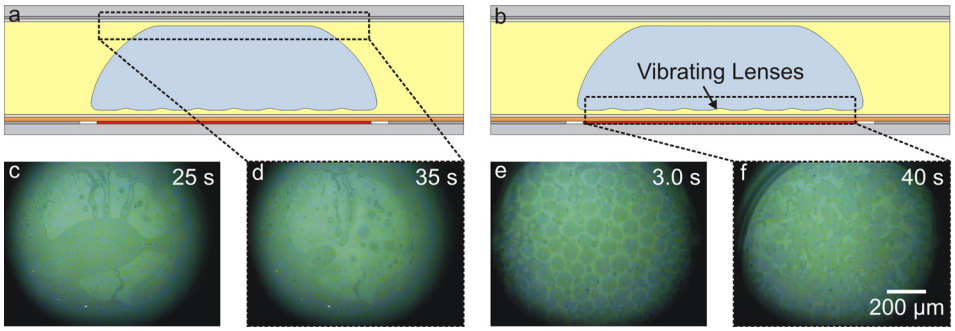

FIG. 6. (a) and (b) Schematic and (c)–(f) interference micrographs showing the evolution of the oil films at (a), (c), and (d) the reference and (b), (e), and (f) the working electrode surfaces when a 10 Hz ac voltage was used to transport droplets instead of a standard 100 Hz ac signal. The droplets vibrated with the lower frequency electric field. (a), (c), and (d) At the reference surface, the vibrations caused the dimple in the center of the film to be squeezed out into the oil meniscus. (b), (e), and (f) At the working electrode surface, the oil lenses vibrated and merged with each other, and the film ruptured.

ranging from 0.0001 to 1.0% (w/v). Films at the working electrode and reference surfaces were observed as droplets were transported forward and backward along a row of electrodes on one cartridge at each level of surfactant. The appearance of the dimple that formed at the reference surface was not affected by the presence of surfactants in either phase. The period of the waves that formed in the film at the working electrode surface during droplet transport decreased as the concentration of surfactant increased, and the oil lenses that subsequently evolved from the waves were smaller in diameter and more numerous, as detailed in Table II and shown in Figure 7. When the surfactant concentration was low, the oil lenses were uniformly distributed up to the edges of the film, and a flat oil film was restored when the voltage was removed, as shown in Figures 7(c) and 7(d), respectively. When the Tween-20 concentration exceeded 0.01% or the Triton X-15 concentration exceeded 0.003%, the lenses occupying a ring around the perimeter of the film were ejected into the oil meniscus, as Figure 7(e) shows. After the voltage was switched off, the interference patterns showed that the annular region of the film without lenses had ruptured, as seen in Figure 7(f). Two concentric contact lines bordered the

TABLE II. Effect of surfactant concentration on droplet-oil interfacial tension and film behavior.

Concentration	Interfacial tension (mN/m)	*Ca*	*Ew*	Average oil lens diameter (μm)	State of film
		(a) Tween 20 added to droplet phase			
0.0003%	42.8	0.70	1.9	92.5	Full of lenses
0.003%	39.4	0.76	2.0	50.8	Full of lenses
0.01%	30.5	0.98	2.6	25.9	Complete draining at perimeter
0.03%	10.9	2.8	7.4	27.8	Complete draining at perimeter
0.1%	6.82	4.4	12	23.7	Complete draining at perimeter
1.0%	7.43	4.0	11	21.8	Complete draining at perimeter
10.0%				19.5	Complete draining at perimeter
		(b) Triton X-15 added to oil phase			
0.0001%	30.0	1.0	2.6	96.3	Full of lenses
0.0003%				92.6	Full of lenses
0.001%	26.4	1.1	3.0	91.4	Full of lenses
0.003%	30.9	1.0	2.6	95.9	Complete draining at perimeter
0.01%	22.8	1.3	3.5	86.7	Complete draining at perimeter
0.03%	11.4	2.6	7.1	71.4	Complete draining at perimeter
0.1%	8.78	3.4	9.1	50.0	Complete draining at perimeter
0.3%				32.4	Complete draining at perimeter
1.0%	8.93	3.4	9.0	35.4—too small to measure	Complete draining at perimeter

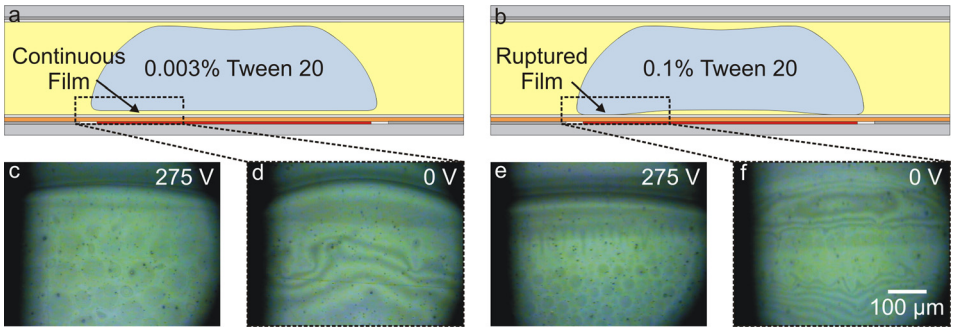

FIG. 7. (a) and (b) Schematics and (c)–(f) interference micrographs showing the evolution of the oil film at the working electrode surface when surfactant (Tween-20) was added to droplets at concentrations of (a), (c), and (d) 0.003% and (b), (e), and (f) 0.1% (w/v). At low surfactant concentrations, (c) lenses were observed up to the edge of the film when voltage was applied, and (d) a continuous film was restored when the voltage was removed. At higher concentrations, (e) lenses were squeezed from the film into the oil meniscus while voltage was applied, and (f) clearly observable contact lines instead of continuous interference patterns at the perimeter of the film after the voltage was switched off indicated that the film had ruptured.

meniscus around the droplet and the film remaining at the center of the droplet. When the actuation voltage was reduced to 100 V, stable oil films were maintained at concentrations of surfactant up to the maximum tested for each type.

IV. DISCUSSION

Many of the experimentally observed static and dynamic features of the films can be interpreted on the basis of fundamental principles of colloids and fluidics. The thermodynamic equilibrium state of the oil wetting films between the water droplets and the microfluidic device surfaces was estimated from the spreading parameter

$$S = \gamma_{WD} - \gamma_{OD} - \gamma_{OW}, \tag{6}$$

where γ_{WD}, γ_{OD}, and γ_{OW} are the water-device, oil-device, and oil-water interfacial energies. For $S > 0$, the oil was expected to completely wet the devices, but for $S < 0$, the water was expected to displace the oil as the oil dewetted to form droplets on the surfaces. Young's equation was used to calculate $\gamma_{WD} = 46$ mN/m and $\gamma_{OD} = 3$ nM/m using contact angles for water and oil of 112° and 39° and surface energies in air for water, oil, and the fluoropolymer cartridge coatings of 73 mN/m, 21 mN/m, and 19 mN/m, respectively. The pendant drop method was used to measure $\gamma_{OW} = 46$ mN/m. Thus, the value of S was estimated to be -3 mN/m, indicating that the oil films were thermodynamically unstable or marginally stable. However, kinetic hydrodynamic effects and disjoining pressure typically also contribute to the stability of thin liquid films.[24,25]

The kinetic film stability was governed by the balance between the capillary pressure from the curvature of the sides of the droplets and the disjoining pressure between the device surfaces and the oil-droplet interfaces. The capillary pressure was given by the equation

$$P_C = \frac{\gamma_{OW}}{R}, \tag{7}$$

where R is the radius of curvature. The value of $R = 160\,\mu$m was calculated based on a contact angle of 160° and a 300 μm gap between the cartridge surfaces, so the capillary pressure was estimated to be 286 Pa. Disjoining pressure is repulsion between the two surfaces of a film arising from van der Waals, electrostatic, and structural forces that are proportional to the area of the film. The forces are assumed to be approximately additive, such that

$$\Pi = \Pi_v + \Pi_e + \Pi_s. \tag{8}$$

Structural forces are typically significant only at length scales of the same order of magnitude as the sizes of the molecules in a film. The molecular weight of the PDMS that comprised the oil was 410 g/mol, corresponding to an average of 8 repeat units and approximate contour length of 2 nm.[26] The interference bands observed in the experiments indicated that the film thickness ranged from 10 to 100 nm. While structural forces were likely insignificant in this system, van der Waals and electrostatic forces were assumed to be operative.

The van der Waals component of the disjoining pressure was estimated from the equation

$$\Pi_v = \frac{A_H}{6\,\pi\,h^3}, \tag{9}$$

where A_H is the Hamaker constant and h is the distance between the film surfaces. The value of $A_H = 3.8 \times 10^{-22}$ J was calculated for the interaction of the droplet and microfluidic device surface across the oil film from the following commonly used approximation[27]

$$A_H \approx \frac{3}{4}\,k\,T\left(\frac{\varepsilon_1-\varepsilon_3}{\varepsilon_1+\varepsilon_3}\right)\left(\frac{\varepsilon_2-\varepsilon_3}{\varepsilon_2+\varepsilon_3}\right)+\frac{3\,h\,\nu_e}{8\sqrt{2}}\frac{\left(n_1^2-n_3^2\right)\left(n_2^2-n_3^2\right)}{\left(n_1^2+n_3^2\right)^{1/2}\left(n_2^2+n_3^2\right)^{1/2}\left[\left(n_1^2+n_3^2\right)^{1/2}+\left(n_2^2+n_3^2\right)^{1/2}\right]}, \tag{10}$$

where k is Boltzmann's constant, T is the temperature, h is Planck's constant, ν_e is the electronic absorption frequency, for which a typical value of 3.0×10^{-15} s^{-1} was used, and ε and n are the dielectric constants and refractive indices for the water, fluoropolymer, and oil phases, denoted as 1, 2, and 3, respectively. The values for ε_1, ε_2, and ε_3 were 80.1, 2.05, and 2.8, and the values for n_1, n_2, and n_3 were 1.33, 1.34, and 1.39. The positive value of A_H indicated that the van der Waals forces were attractive and destabilizing, and the contribution to the disjoining pressure increased as the film thickness decreased and ranged from 0.020 to 20 Pa for films of 10–100 nm thickness using the estimated Hamaker constant. Retardation effects can result in significantly lower dispersion forces, accounted for by the second term in Eq. (10), when the phases are separated by distances of approximately 10 nm or greater, as expected for the oil films in this system. However, the calculations showed that at any degree of retardation, van der Waals forces had only a minute contribution to the total disjoining pressure required to balance the capillary pressure calculated above.

The electrostatic component of the disjoining pressure arose from osmotic pressure from counterions in the film balancing charges at the film surfaces and was given by

$$\Pi_e = k\,T\,\rho_0, \tag{11}$$

where ρ_0 is the concentration of counterions at the midplane of the film.[27] The film thickness h was directly related to the surface charge σ using a solution of the Poisson-Boltzmann equation

$$\sigma = \frac{-1}{\varepsilon_f\,\varepsilon_0}\left(\frac{2\,k\,T\,K}{z\,e}\right)\tan\left(\frac{K\,h}{2}\right), \tag{12}$$

in which ε_f is the dielectric constant of the film, z is the ion valency, e is the charge of an electron, and

$$K^2 = \frac{(z\,e)^2\rho_0}{2\,\varepsilon\,\varepsilon_0\,k\,T}. \tag{13}$$

While the oil was considered nonpolar, accumulation of only a small number of charges at the film surfaces could have engendered significant repulsion. Using Eqs. (11)–(13) and assuming $T = 298$ K and $z = 1$, a repulsive pressure sufficient to sustain a film thickness of 32.0–33.6 nm against a capillary pressure of 286 Pa would have been provided by a density of one charge per

1–100 nm^2. Thus, charging at the film interfaces might explain how oil films were stabilized in the DMF devices.

Additional factors affected the film stability during electrowetting-driven droplet transport. The capacitive energy engendered by applying voltage across the film gave rise to an effective electrostatic pressure between the oil-water and dielectric-working electrode interfaces that caused the film to thin. The energy from the voltage driving electrowetting was calculated using the equation

$$E_{EW} = \frac{\varepsilon_d \, \varepsilon_0 \, V^2}{2 \, d}, \tag{14}$$

which was valid as long as $d \gg h$.[8,21,22] The destabilizing surface energy due to the applied voltage was 12 mN/m at $V = 100$ V but increased to 93 mN/m at $V = 275$ V. The relative magnitudes of these energies may partially explain why the oil film remained stable with droplet actuation at 100 V but broke up into lenses when the voltage was increased to 275 V.

Translational motion of droplets caused oil to be entrained in the films, opposing the tendency of the films to thin under applied voltage. The effect of droplet motion on films was described by the Landau-Levich theory, whereby the thickness of a wetting film trailing behind a receding meniscus increased with the speed of the meniscus according to Eqs. (1) and (2). In an earlier work, the speed of droplets in DMF devices was determined to follow the relation

$$\frac{\varepsilon_d \, \varepsilon_0}{2d} \left(V^2 - V_T^2 \right) = B \left(\frac{\mu_W \, U}{\gamma_{OW}} \right)^{0.3} \gamma_{OW} + \left(\frac{m \, L}{H} + s \right) \mu_O \, U + \zeta \, U, \tag{15}$$

where V_T is the threshold voltage at which the droplet overcomes contact angle hysteresis, μ_W and μ_O are the viscosities of the water and oil, L is the electrode pitch, H is the distance between the top and bottom surfaces of the device, and B, m, s, and ζ are empirically determined parameters.[28] The left side of the equation describes the electrowetting force that moves the droplet, while the terms on the right side describe the resistance due to flow inside the droplet, oil flow around the droplet, and interfacial molecular phenomena including surface tension gradients, respectively. Consistent with the experimental observations, the model predicted that the droplet speed would increase with applied voltage, which, according to the Landau-Levich theory, would also increase the film thickness.

A simple scaling analysis could explain the relative magnitudes of the hydrodynamic and electrical effects on the film behavior across the range of voltages examined in the experiments. Increasing the applied voltage increased the capacitive energy that resulted in thinner films. As Eq. (14) indicated, $E_{EW} \sim V^2$. The speed of the droplets also increased with the voltage, as described by Eq. (15). The displacement of oil was the dominant force resisting droplet motion, so the first and last terms from the right hand side of the equation were neglected. The remaining terms yielded $U \sim V^2$. The amount of oil driven into the film and the film thickness increased with the droplet speed such that $h \sim U^{2/3}$, according to Eqs. (1) and (2). Thus, $h \sim V^{4/3}$. The response to an increase in the voltage was greater for the electrostatic pressure than for the film thickening arising from the droplet motion. Therefore, the fluid dynamic effects may have been dominant so that the height of the film increased when a droplet was transported at low voltage, but the electrostatic pressure may have become dominant at high voltage and caused the formation of oil lenses.

When the voltage was switched off after transporting a droplet by electrowetting, the oil lenses that had formed at the working electrode surface disappeared and a continuous film was restored in most experiments. However, when the ac frequency was low or the surfactant concentration was high, contact lines were visible between the droplet and the working electrode surface, indicating that the film was broken. Both outcomes may be interpreted according to the hypothesis that the oil film was kinetically stabilized but thermodynamically unstable. In the instances in which the film was observed to be ruptured, the energy provided upon applying voltage was sufficient to overcome the disjoining pressure and hydrodynamic film thickening

effects. Once the droplet directly contacted the device surface, the system achieved a permanent, thermodynamically favored state. Thus, in the other experiments, the tendency of the oil film to rewet the device surface after the voltage was removed suggested that a thin residual layer of oil may have continually remained between the oil lenses while the voltage was applied.

A more detailed theory for film destabilization during electrowetting was developed by Staicu and Mugele, who described entrapment and subsequent spinodal decomposition of oil films after voltage was applied across a sessile droplet in an oil medium on a dielectric-covered electrode.[22] In the droplet transport experiments performed during this investigation using 175 V and higher voltages, the diameter of the oil lenses at the working electrode surface d_{lens} followed the relations $d_{lens} \sim \gamma_{OW}$ and $d_{lens} \sim 1/V$, consistent with the model developed by Staicu and Mugele for the wavelengths of the oscillations in the films. However, the results of the droplet transport experiments performed at 100 V diverged from those of the earlier sessile droplet experiments. The electrostatic pressure, proportional to V^2/d, was equivalent for both systems, as the dielectric thickness was 13 μm in the droplet transport experiments and the voltage and dielectric thickness were 25 V and 0.8 μm in the sessile droplet experiments. However, the speed of the receding oil meniscus differed between the two systems. In the sessile droplet experiments, the voltage was ramped slowly from 0 to 25 V to control the rate of droplet spreading, and the maximum speed of the meniscus was approximately 0.6 mm/s. In the droplet transport experiments, the electrodes were switched instantaneously from 0 V to 100 V, and the speed of the meniscus was 1.5 mm/s. The speed of the meniscus may have been high enough that the fluid dynamic effects thickened the film when transporting droplets at 100 V, where the electrostatic pressure was weak. At high voltage, where the electrostatic pressure was dominant, the films evolved into lenses at all meniscus speeds by the mechanism described by Staicu and Mugele. The comparison of these two experimental outcomes reiterates that DMF devices should be operated at low voltage to maintain stable oil films.

The dimple of oil at the reference surface was formed by a different mechanism than the oil lenses in the film at the working electrode surface. During transport, the droplet became momentarily elongated as the leading end rapidly wetted the activated electrode. The stretched droplet was pulled away from the top plate to conserve its volume. As the droplet moved onto the energized electrode, it reassumed its original disk shape and reapproached the top plate. The radial flow of oil out of the gap between the droplet and the top plate was faster at the perimeter of the droplet than at the center. The pressure normal to the droplet surface was proportional to the velocity of the oil. The resulting pressure gradient and nonuniform rate of film thinning led to trapping of a thick oil film in the center of the droplet and formation of a dimple. Similar dimpling phenomena have been well characterized by other researchers studying droplets moving perpendicularly to flat, nondeformable surfaces.[25]

Film instabilities were caused by oscillations in the surfaces of the droplets at some ac frequencies. The oscillations were driven by the droplets spreading to the corners of the square working electrodes at the peaks of each ac voltage cycle and returning to a relaxed circular shape when the voltage passed through zero. Propagation of the oscillations may have been partially limited by the microfluidic device surfaces, which constrained the movement of the tops and bottoms of the droplets, in contrast to devices with open geometries that allow the tops of the droplets to vibrate freely. Consistent with the occurrence of the strongest droplet shape oscillations at 10 Hz ac frequency, previous researchers found that the amplitudes of droplet shape oscillations associated with electrowetting were highest at specific resonant frequencies but tended to decrease with increasing ac frequency as the vibrations were damped by the surrounding oil.[29–32] The oscillations drove waves on the surfaces of the droplets and engendered flows inside the droplets that promoted mixing. The rupturing of the films observed in the experiments using 10 Hz ac frequency was believed to be caused by oscillations in the free interfaces of the films reaching sufficient amplitude that the droplets contacted the device surfaces. Such oscillations may lead to film instability at other resonant frequencies not tested in these experiments.

The hypothesis considered most likely to explain the surfactant-concentration dependence of the stability of oil films in DMF devices was based on the tendency for a surface tension gradient to be sustained along the oil-droplet interface. Trace surfactants were expected to be ever present as general contaminants and residuals of the cartridge and oil manufacturing processes. These molecules may have adsorbed to the oil-droplet interface and caused film thickening by the Marangoni effect during droplet transport as described in the introduction. Deliberate addition of surfactant to the droplets or oil may have suppressed the concentration gradients that led to film thickening if the additional bulk surfactant molecules adsorbed rapidly to the regions of the interface depleted of surfactants by the liquid flow. Thus, increasing the surfactant concentration may have caused the films at the working electrode surface to break more readily, as observed during the experiments, because contact between the free interface and aberrations on the device surfaces would have been more likely with less distance between them. The annular pattern of the breakup of the films was hypothesized to result from the dimpling phenomenon described in the previous paragraph. A radial pressure gradient may have been present in the thinning film at the working electrode surface just like at the reference surface. For systems without surfactant added, dimple formation may not have been apparent at the working electrode surface because the gap between the device surface and the droplet during transport was much smaller than at the reference surface. Adding surfactant reduced the oil-droplet interfacial tension and may have made the droplet surface more deformable and responsive to the pressure gradient created by the flow of oil out of the film. Therefore, with increasing surfactant concentration, the film at the working electrode surface may have become thinner and more likely to rupture, and, due to the dimpling effect, the difference in the height of the film between the center and perimeter of the droplet may have become large enough that the edge of the film ruptured first and trapped oil inside the ring. Based on the experimental observations, minimizing the concentration of surfactant added to the system is desirable for maintaining stable lubricating films.

V. CONCLUSIONS

The results of this investigation provide numerous insights into the dynamics and stability of oil films lubricating transport of water droplets by electrowetting in commercial digital microfluidic devices. Before the actuation voltage was applied, thin but continuous oil films isolated the droplets from the device surfaces. The films may have been stabilized by a small amount of charge adsorbed to the interfaces. After the voltage was switched on, the droplets spread to cover the working electrode surfaces, expanding the area of the films. The dynamics of the oil films during droplet movement were determined by the balance of the competing effects of electrostatic pressure, which made the films thinner as the voltage increased, and liquid entrainment at the receding oil meniscus, which increased the film thickness as the droplet speed increased. At low voltage, the electrostatic pressure was small relative to the liquid entrainment, and the films remained intact during droplet transport. At high voltage, the electrostatic pressure became dominant, and the films degenerated into arrays of oil lenses. A single, central dimple of oil formed between the top of each droplet and the device surfaces. The dimples were caused by a radial pressure gradient that arose in the oil films due to droplet deformation during transport. The films at both surfaces were ruptured by low-frequency actuation voltage that induced droplet vibrations and by addition of surfactants to the droplet or the oil. Traces of surfactants at the droplet surfaces were believed to become non-uniformly distributed during transport, giving rise to interfacial tension gradients that forced oil into the films by the Marangoni effect. Surfactant additives may have suppressed the gradients that led to film thickening and made the oil-droplet interfaces more deformable, possibly explaining why the films were observed to rupture around the edges of the droplets.

The observed film phenomena have important implications for the implementation of assays using digital microfluidics. To achieve useful speed and throughput in practical DMF devices, many droplets must travel over the same areas on the cartridge surfaces. Maintaining acceptable sensitivity and precision depends on inhibiting carryover of species between

droplets. The insights from this study can be used to select conditions under which continuous oil films are maintained to prevent adsorption and desorption of molecules such as proteins or DNA to and from the device surfaces. The data point out that as low voltage as possible should be used to actuate droplet transport to minimize the electrostatic pressure that thins the films and that can cause spinodal decomposition. The ac frequency should be selected to avoid droplet resonance that can cause the films to rupture; in particular, low frequencies at which droplet oscillation amplitudes tend to be largest are not recommended. Although often necessary for assay performance, the addition of surfactants to the droplet or oil phases was found to be undesirable from the perspective of oil film stability. The introduction of new classes of surfactants, coatings, or filler fluids that will improve the film stability and enhances the wettability of the device surfaces by oil instead of water would be an important next goal in the future development of more robust DMF devices.

ACKNOWLEDGMENTS

The authors are grateful for support for this research from the U.S. National Science Foundation (CBET Grant 0828900 and NSF-ASSIST NERC Grant EEC-1160483) and the U.S. National Institutes of Health (NHLBI Grant HHSN268201000001C). Additional support was provided by the NCSU/NIH Molecular Biotechnology Training Program. The content is solely the responsibility of the authors and does not necessarily represent the official views of the National Institutes of Health.

[1]R. B. Fair, A. Khlystov, T. D. Tailor, V. Ivanov, R. D. Evans, P. B. Griffin, V. Srinivasan, V. K. Pamula, M. G. Pollack, and J. Zhou, IEEE Des. Test Comput. **24**, 10–24 (2007).
[2]M. G. Pollack, V. K. Pamula, V. Srinivasan, and A. E. Eckhardt, Expert Rev. Mol. Diagn. **11**, 393–407 (2011).
[3]W. C. Nelson and C.-J. Kim, J. Adhes. Sci. Technol. **26**, 1747–1771 (2012).
[4]M. J. Jebrail, M. S. Bartsch, and K. D. Patel, Lab Chip **12**, 2452–2463 (2012).
[5]M. G. Pollack, A. D. Shenderov, and R. B. Fair, Lab Chip **2**, 96–101 (2002).
[6]M. G. Pollack, R. B. Fair, and A. D. Shenderov, Appl. Phys. Lett. **77**, 1725–1726 (2000).
[7]O. D. Velev, B. G. Prevo, and K. H. Bhatt, Nature **426**, 515–516 (2003).
[8]F. Mugele and J.-C. Baret, J. Phys.: Condens. Matter **17**, R705–R774 (2005).
[9]A. B. Theberge, F. Courtois, Y. Schaerli, M. Fischlechner, C. Abell, F. Hollfelder, and W. T. S. Huck, Angew. Chem. Int. Ed. **49**, 5846–5868 (2010).
[10]V. Srinivasan, V. K. Pamula, and R. B. Fair, Lab Chip **4**, 310–315 (2004).
[11]D. Chatterjee, H. Shepherd, and R. L. Garrell, Lab Chip **9**, 1219–1229 (2009).
[12]D. R. Link, E. Grasland-Mongrain, A. Duri, F. Sarrazin, Z. Cheng, G. Cristobal, M. Marquez, and D. A. Weitz, Angew. Chem. Int. Ed. **45**, 2556–2560 (2006).
[13]L. Landau and B. Levich, Acta Phys. Chim. URS **17**, 42–54 (1942).
[14]F. P. Bretherton, J. Fluid Mech. **10**, 166–188 (1961).
[15]L. Y. Yeo and H.-C. Chang, Phys. Rev. E **73**, 011605 (2006).
[16]L. W. Schwartz, H. M. Princen, and A. D. Kiss, J. Fluid Mech. **172**, 259–275 (1986).
[17]S. R. Hodges, O. E. Jensen, and J. M. Rallison, J. Fluid Mech. **501**, 279–301 (2004).
[18]J. Ratulowski and H.-C. Chang, J. Fluid Mech. **210**, 303–328 (1990).
[19]K. J. Stebe and D. Barthès-Biesel, J. Fluid Mech. **286**, 25–48 (1995).
[20]K. J. Stebe, S.-Y. Lin, and C. Maldarelli, Phys. Fluids A **3**, 3–20 (1991).
[21]C. Quilliet and B. Berge, Europhys. Lett. **60**, 99–105 (2002).
[22]A. Staicu and F. Mugele, Phys. Rev. Lett. **97**, 167801 (2006).
[23]A. Sheludko, Adv. Colloid Interface Sci. **1**, 391–464 (1967).
[24]B. Derjaguin and E. Obuchov, Acta Phys. Chim. URS **5**, 1 (1936).
[25]I. B. Ivanov and D. S. Dimitrov, *Thin Liquid Films* (Dekker, New York, 1988).
[26]R. Gill, M. Mazhar, O. Félix, and G. Decher, Angew. Chem. **122**, 6252–6255 (2010).
[27]J. N. Israelachvili, *Intermolecular and Surface Forces*, 2nd ed. (Academic Press, London, 1991).
[28]H. Ren, R. B. Fair, M. G. Pollack, and E. J. Shaughnessy, Sens. Actuators, B **87**, 201–206 (2002).
[29]R. Malk, A. Rival, Y. Fouillet, and L. Davoust, in *Proceedings of the 8th International Conference on Nanochannels, Microchannels, and Minichannels*, Montreal, Canada, 1–5 August 2010 (American Society of Mechanical Engineers, New York, 2010), pp. 239–248.
[30]F. Mugele, A. Staicu, R. Bakker, and D. van den Ende, Lab Chip **11**, 2011–2016 (2011).
[31]L. Davoust, Y. Fouillet, R. Malk, and J. Theisen, Biomicrofluidics **7**, 044104 (2013).
[32]C.-P. Lee, H.-C. Chen, and M.-F. Lai, Biomicrofluidics **6**, 012814 (2012).